International Journal of Heat and Mass Transfer 78 (2014) 267–276

Contents lists available at ScienceDirect

International Journal of Heat and Mass Transfer

journal homepage: www.elsevier.com/locate/ijhmt

Droplet breakup of micro- and nano-dispersed carbon-in-water colloidal suspensions under intense radiation

Jian Xu [a], Li Qiao [a,*], Jian Gao [b], Jun Chen [b]

[a] School of Aeronautics and Astronautics, Purdue University, West Lafayette, IN 47907, United States
[b] School of Mechanical Engineering, Purdue University, West Lafayette, IN 47907, United States

ARTICLE INFO

Article history:
Received 13 January 2014
Received in revised form 19 June 2014
Accepted 23 June 2014
Available online 22 July 2014

Keywords:
Carbon-in-water suspensions (CWS)
Droplet breakup
Mie scattering
Radiation-intensity threshold

ABSTRACT

Carbon-in-water suspensions (CWS) have unique optical properties and have received increasing interest recently for various applications. In the field of combustion science, CWS have been recommended as a substitute for the traditional fossil fuels. The idea is to suspend carbon (coke or coal) particles in water and then inject them as a spray into a gasifier or boiler. The potential benefits are lower emissions and higher combustion efficiency, in comparison to directly injecting coal particles into air or water steam. Nevertheless, few studies have examined CWS colloidal fuels. Especially, droplet breakup can occur when the droplets are exposed to radiation. The goal of this paper is to understand droplet breakup mechanism of CWS under intense radiation. An experiment was developed to visualize the breakup process and to measure the threshold radiation intensity required for explosion at varying particle concentrations and sizes as well as droplet sizes. The results show that radiation absorption by the carbon particles play a critical role in the breakup behavior. A theoretical model was also developed to determine the effects of the particle material, size, and concentration on the threshold radiation energy.

1. Introduction

Carbon-in-water suspensions (CWS) have unique optical properties and have attracted great interest recently for various applications. For example, they can be used as a nonlinear optical limiter, a protective device whose transmission is rapidly decreased with increasing of the incident radiation [1]. In the combustion field, carbon (coke or coal)-in-water suspensions have been recommended as a substitute for traditional fossil fuels for use in boilers and gasifiers. Because of its low emissions and low BTU costs, CWS can be environmental friendly and cost-effective for heat and power generation [2]. Nevertheless, few studies have examined CWS colloidal fuels. Especially, droplet breakup can occur when the droplets are exposed to radiation.

Radiation-induced droplet breakup of pure liquids or liquid mixtures has been studied previously [3–5]. The mechanism is well understood, especially for water droplets: the high intensity radiation from a laser produces a plasma; unlike water which is almost transparent to the incident radiation, the plasma absorbs much of the laser energy and converts it to heat; explosion takes place when the superheating temperature of the liquid nearby the plasma is reached. However, there are fewer studies on the breakup of colloidal suspensions under radiation (explosive boiling) [6–8], for which the breakup mechanism is completely different from that of pure liquids.

Explosive boiling has been observed for aluminum slurry [9], aluminum nanofluid [10], and coal–oil mixtures [11]. Maloney and co-workers [6–8] studied the explosive boiling behavior of CWS droplets, in which radiation was generated by a pulsed Nd:YAG laser with 1064 nm wavelength and a heating time of around 8 ms. It was proposed that the internal superheating and explosive boiling were caused by the fuel additives (the surfactant), which formed a thin film at the droplet surface [7]. The other study [8], however, suggested that the breakup was caused by the coal particles in the outer layer of the CWS droplet absorbing radiation energy, and the heat was then transferred inward through internal conduction causing droplet breakup.

Note all previous studies used coal particles of a size in the range of submicrons to a few hundred microns. Recently, nano-dispersed coal-in-water colloidal fuels have received increasing interest. They are nonsettling colloidal dispersions of nano-sized carbonaceous materials with water and have shown outstanding long-term stability, high combustion efficiency, and less soot formation [12]. No studies have examined the radiation-induced droplet breakup of nano-dispersed colloidal fuels. We believe that

* Corresponding author.
E-mail address: lqiao@purdue.edu (L. Qiao).

http://dx.doi.org/10.1016/j.ijheatmasstransfer.2014.06.068
0017-9310/

the size of the coal particles suspended in water plays a vital role in the explosive boiling behavior.

The objective of this study is to understand the mechanisms that are responsible for the radiation-induced droplet breakup of micro- and nano-dispersed CWS, especially the influence of carbon particle size. An experiment was developed to visualize the droplet breakup process and to measure the threshold radiation energy (or flux) under various conditions (droplet diameter, and particle size and concentration). Moreover, a theoretical model was developed to further understand the mechanism of radiation-induced droplet breakup and to determine the effects of the particle material, size, and concentration on the threshold radiation energy and the explosive boiling behavior.

2. Experimental method

2.1. Fuel preparation and morphology

Carbon particles of three different kinds were selected and mixed with water to generate CWS colloidal fuels: (a) diamond particles with a mean diameter of 6 nm; (b) activated carbon particles with a mean diameter of 100 nm; and (c) graphite particles with a mean diameter of 20 μm. Fig. 1 shows the Scanning Electron Microscope (SEM) photographs of these particles. For 6-nm and 100-nm particles, their shapes are mostly spherical, and the sizes are nearly uniform. For 20-μm particles, they have a size range of 1–35 μm and are more random in shape.

The carbon particles were dispersed into water using an ultrasonic disruptor (Sharpertek, SYJ-450D). It delivered a series of 4-s-long pulses 4 s apart to disperse particles evenly and to reduce agglomeration. It was turned on for about 6 min for each CWS sample. In this study, we added no surfactant, which could have enhanced the chemical stability of the colloidal suspensions. This was because adding a surfactant complicates the understanding of the mechanism that causes explosion. However, the experiments were conducted shortly after the fuel was prepared; thus the influence of particle agglomeration was minimized. A syringe pump running at a low flow rate was used to generate a droplet at a desired size (the range of the droplet size is 0.9–2.0 mm). The droplet was then transferred to the suspension point by another syringe.

2.2. Experimental setup

The schematic of the experiment is shown in Fig. 2. The CWS droplet was suspended on a silicon carbide (Si-C) fiber with a diameter of 70 μm. The droplet evaporation and explosion processes were recorded by a high-speed digital video camera (Phantom V7.3, Vision Research). A microlens was coupled with the camera to capture the magnified view of the droplet, and an LED light was also used to provide backlight for the camera.

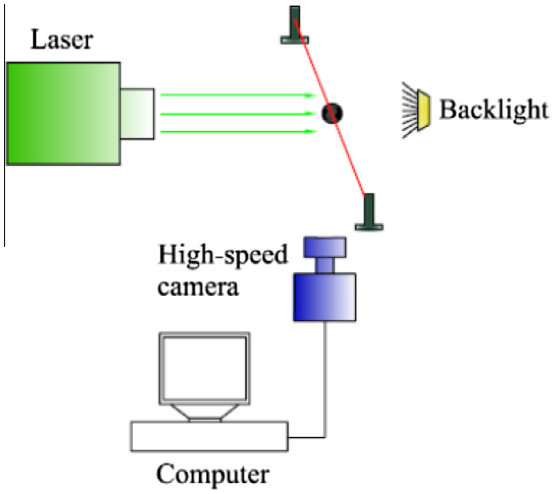

Fig. 2. Schematic of the experiment setup for radiation-induced explosive boiling of CWS fuels.

A dual-pulsed Nd:YAG laser (Evergreen 200, Quantel) with a 532-nm wavelength and 10-ns pulse width was used to irradiate the CWS droplet. At the visible wavelength, the water is weakly absorbing so that most of the radiation energy is absorbed by the particles in the droplet. The highest pulse energy of the laser is 200 mJ. The pulse energy can be adjusted from the front panel of the laser and by altering the time delay between the Q-switch and the flash lamp. The energy level from the laser was confirmed by measuring the beam energy, using an energy meter. The laser provided flattop and uniform near-field beam with a diameter of about 6.35 mm. In the experiment, the laser was controlled to last only one pulse. Therefore the heating time was fixed at 10 ns. The thresholds were determined by gradually increasing the energy intensity until the explosive fragmentation was reached. If no fragmentation had been achieved at a certain energy intensity, a new droplet with the same size was used for the next round of irradiation with increased energy intensity.

3. Theoretical modeling

3.1. Fundamental mechanism of radiation-induced colloidal droplet breakup

When a colloidal droplet is exposed under a collimated laser beam, the particles inside the droplet will move as a result of the photophoretic force. Following Tong's photophoresis model

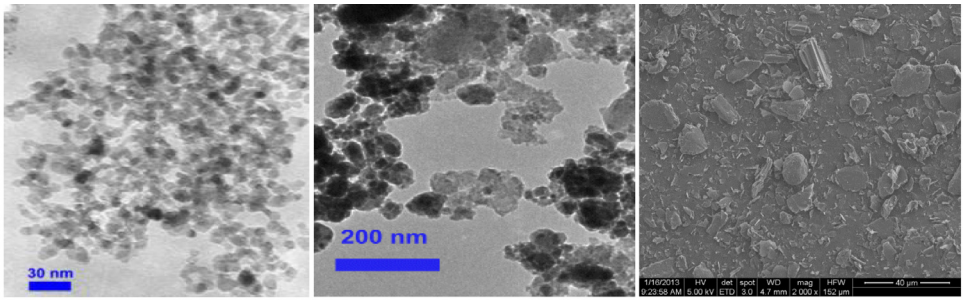

(a) diamond: 6 nm **(b) activated carbon: 100 nm** **(c) graphite: 20 μm**

Fig. 1. SEM photographs of different carbon particles: (a) diamond particles, 6 nm; (b) activated carbon particles, 100 nm; and (c) graphite particles, 20 μm.

[13,14], we found that the displacement of the particles inside the droplet is negligible because the laser pulse is as short as 10 ns and the particle size is small (from a few nanometers to a few microns). Therefore during the 10-ns radiation process, the particles were still uniformly distributed within the droplet.

We propose the following theoretical model to simulate the breakup process as shown in Fig. 3. The laser beam is first scattered and absorbed by the spherical droplet. The light that enters the droplet is further scattered and absorbed by the particles inside the droplet. Since the breakup initiates from the illuminated side of the droplet in our study, we can choose any particle in this location to represent the thermal interaction between the particle and the surrounding water. The heat transfer between the two, taking place through a very thin thermal resistance layer (on the order of nanometers), is mainly a result of thermal conduction. Breakup takes place when the temperature of the surrounding water exceeds its maximum superheat temperature at given pressures.

Based on these assumptions, the modeling of the laser-induced droplet breakup process can be divided into three steps:

(1) Calculate the effective complex refractive index of the droplet (a two-phase mixture), using Bruggeman's effective medium theory.
(2) Determine the absorption efficiency of the droplet and that of a single particle inside the droplet, using the Mie scattering theory.
(3) Compute the temperatures of the particle and its surrounding water using thermal interface conductance model.

3.2. Effective medium theory

As the first step, Bruggeman's effective medium theory [15,16] was used to calculate the complex refractive index of the droplet, which can then be applied to compute the radiation absorption by the droplet, using the Mie scattering theory. The effective complex refractive index of a two-phase mixture is expressed as a function of the volume fractions and the complex refractive indices of the particles and the liquid, as shown in Eq. (1)

$$n_1\frac{m_1^2-m_{eff}^2}{m_1^2+2m_{eff}^2}+(1-n_1)\frac{m_2^2-m_{eff}^2}{m_2^2+2m_{eff}^2}=0 \tag{1}$$

where n_1 is the volume fraction of the particles inside the droplet, and m_1, m_2, and m_{eff} are the complex refractive indices of the particle, liquid, and effective medium, respectively.

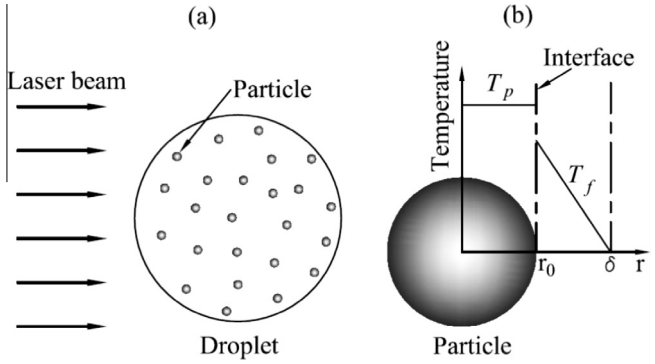

Fig. 3. Schematic of the droplet breakup modeling processes: (a) the laser beam will be successively scattered and absorbed by the droplet and particles; (b) thermal interface conductance is used to calculate the heat diffusion from one particle to the surrounding water.

3.3. Mie scattering theory

The sizes of studied particles ranged from a few nm to 25 μm. The scattering of light by the particles whose size is on the same order of light wavelength can be determined by the Mie scattering theory developed by Mie [17], which is an exact solution to Maxwell's equations and can be used to calculate the scattering of electromagnetic radiation by a sphere. The scattering efficiency (Q_{sca}), the extinction efficiency (Q_{ext}), and the absorption efficiency (Q_{abs}) can be obtained by the equations below [18],

$$Q_{sca}=\frac{2\pi}{x_2}\Sigma_{n=1}^{\infty}(2n+1)(|a_n|^2+|b_n|^2) \tag{2}$$

$$Q_{ext}=\frac{2\pi}{x_2}\Sigma_{n=1}^{\infty}(2n+1)Re\{a_n+b_n\} \tag{3}$$

$$Q_{abs}=Q_{ext}-Q_{sca} \tag{4}$$

where x is the size parameter and is equal to $\frac{\pi D_p}{\lambda}$, D_p is the diameter of the scattering sphere, and λ is the wavelength in the ambient medium; a_n and b_n are the Mie coefficients and are expressed as

$$a_n=\frac{\mu m^2 J_n(mx)[xj_n(x)]'-\mu_1 j_n(x)[mxj_n(mx)]'}{\mu m^2 J_n(mx)\left[xh_n^{(1)}(x)\right]'-\mu_1 h_n^{(1)}(x)[mxj_n(mx)]'} \tag{5}$$

$$b_n=\frac{\mu_1 J_n(mx)[xj_n(x)]'-\mu j_n(x)[mxj_n(mx)]'}{\mu_1 J_n(mx)\left[xh_n^{(1)}(x)\right]'-\mu h_n^{(1)}(x)[mxj_n(mx)]'} \tag{6}$$

where m is the complex refractive index of the sphere relative to the ambient medium; j_n is the spherical Bessel function; and $h_n^{(1)}$ is the first kind Hankel function.

Mätzler's MATLAB functions for Mie scattering and absorption [19] were adopted to calculate the absorption efficiency (Q_{abs}). First, a droplet of the carbon–water mixture was considered as the scattering sphere, and the effective complex refractive index of the droplet obtained previously was used to calculate its absorption efficiency ($Q_{abs,d}$). Second, a single carbon particle in the droplet was chosen, and its absorption efficiency ($Q_{abs,p}$) can be calculated by again using the Mie scattering theory. This method is valid when the scattering of the particle can be assumed to be independent scattering, and this assumption is also valid in this work because we controlled the concentration of the particles. This will be discussed in detail in Section 4.3.

3.4. Thermal model

The radiation energy from the laser is mostly absorbed by the particles. The water surrounding the particles is then heated up through thermal conduction. Following the method from [20,21], we assumed a finite thermal interface conductance between the solid phase and the fluid phase.

The energy equations for the particle and the surrounding media are

$$m_p C_{p,p}\frac{dTp}{dt}=\dot{Q}_{rad}-\dot{Q}_{cond} \tag{7}$$

$$\frac{\partial T_f}{\partial t}=\frac{K_f}{C_{p,f}\rho_f}\frac{\partial^2 T_f}{\partial r^2} \tag{8}$$

where the subscript p and f denote the particle and the surrounding water; m, T, C_p, K, and ρ are the mass, temperature, heat capacity, thermal conductivity, and density, respectively. C_p and K are both functions of the temperature; $\dot{Q}_{rad}$ is the radiation energy flux that is absorbed by the particle; and $\dot{Q}_{rad}=\pi r_0^2\cdot I_0 Q_{abs,d}Q_{abs,p}$, I_0 is the initial laser energy flux; $\dot{Q}_{cond}$ is the heat diffusion from the particle to the surrounding media through thermal conduction and is expressed as $\dot{Q}_{rad}=4\pi r_0^2\cdot G(T_p-T_f)|_s$, G is the thermal conductance

at the carbon–water interface. A value of 10^3 W/cm^2 K for G was adopted in this study according to Refs. [22,23].

The interface equation is

$$-K_f \frac{\partial T_f}{\partial t}\bigg|_s = G(T_p - T_f)|_s \tag{9}$$

where the subscript s denotes the interface between the two phases.

The droplet breakup is assumed to take place when the fluid temperature at the interface reaches 578 K, and the radiation-intensity threshold is determined as the minimum I_0 required to cause droplet breakup.

3.5. Computational method

The above equations which describe the droplet breakup mechanism under intense radiation were numerically solved using MATLAB. The optical equations (Eqs. (2)–(6)) were solved by Mätzler's MATLAB functions for Mie scattering and absorption [19] to calculate the absorption efficiency (Q_{abs}). The governing equations for the particle (Eq. (7)) and the surrounding water (Eq. (8)) and the boundary equation (Eq. (9)) were discretized on the one-dimensional thermal boundary layer around the particle. The resulting discretized system was then solved by the Crank–Nicolson scheme which has second-order accuracy [24]. A thin thermal boundary layer on the particle surface was assumed. Its thickness was set to be $0.05d_p$ for each particle, where d_p is the diameter of the particle. Other thicknesses were also tested and the results were similar.

4. Results and discussion

4.1. Radiation-induced droplet breakup process

The breakup behavior of CWS droplets with a diameter in the range of 0.9–2.0 mm was studied. The droplet explosion process is shown in Fig. 4; the carbon particles have a mean diameter of about 20 μm and the particle concentration is 1 wt%. The droplet was suspended on a fiber that was placed perpendicular to the plane of the paper. The laser beam was from right to left. Its diameter was 6.35 mm, and the entire droplet was covered within the beam.

The breakup takes place on the illuminated side, where most of the radiation energy is absorbed by the carbon particles in that area. Although the irradiation time is only 10 ns, the explosion takes about 0.035 ms to begin. After about 0.2 ms, many small droplets are observed to be ejected from the original droplet. After 3 ms, some big droplets will also be generated in the later phase of the explosion. The breakup processes of droplets with 6-nm and 100-nm particles are similar to those with 20-μm particles shown in Fig. 4.

Pure water droplets (no particles added) were also tested. They can breakup under higher radiation intensities (10 times higher than the intensities required for the CWS droplets to breakup). The breakup starts from the center of the droplet and is caused by heating of the fiber which was used to suspend the droplet. Note this breakup mechanism is also different from those of micron-sized water droplet without the use of a fiber in previous studies. This is summarized in Table 1. In Ref. [5], the breakup of a water droplet illuminated by a laser with 0.532 μm wavelength and 10 ns duration happens on the shadow face, while in Ref. [3], the water droplets explode on the illuminated side under the irradiation of a laser with 10.591 μm wavelength and 400 ns duration. The different location of the droplet breakup in [3,5] is because of the different peak heating location caused by the plasma absorption.

The fiber effect, however, is negligible for the breakup of CWS droplets in the present study because on the one hand, the radiation intensity required to cause the breakup of pure water droplets (in the order of 10^9 W/cm^2) is much higher than that for CWS droplets; on the other hand, as observed in the experiments, the explosion only takes place in the frontal part of the droplet as a result of irradiation from the laser beam. Therefore, we can conclude that the droplet breakup is mainly caused by the radiation absorption by the particles in the frontal part of the droplet.

4.2. Measured radiation-intensity threshold

Fig. 5 shows the radiation-intensity threshold required for explosive boiling to happen for droplets with 1 wt% carbon particles as a function of droplet diameter for three different particle sizes. Note that only one laser pulse was generated, and the pulse duration was fixed at 10 ns for all conditions, which means the heating time was 10 ns for all instances. It can be seen from Fig. 5 that the radiation intensity threshold for CWS droplets with 1 wt% carbon changes only slightly with the droplet diameter. However, it changes significantly with the carbon-particle size. An average value of the radiation intensity is around 4.8×10^8 W/cm^2, 9×10^7 W/cm^2, and 1.7×10^8 W/cm^2 for particle sizes of 6 nm, 100 nm, and 20 μm, respectively. The droplets with 100-nm particles require the lowest radiation intensity for breakup to occur; the reason will be explained in the following section.

The radiation-intensity threshold was also measured for droplets with different particle concentrations. The results for 100-nm and 20-μm particles are shown in Figs. 6 and 7. Fig. 6 shows that for the droplets with 100 nm nanoparticles, the radiation-intensity threshold remains nearly constant. In other words, it does not depend on the particle concentration. We can draw a similar conclusion for droplets with 20-μm particles at particle concentrations of 1 wt% and 5 wt%, as shown in Fig. 7. However, the radiation-intensity threshold slightly decreases from 1.65×10^8 W/cm^2 to 1.15×10^8 W/cm^2 when the particle concentration increases from 5 wt% to 10 wt%. This is likely because for higher particle concentration, the multiple scattering effect will become more significant, which leads to a lower radiation-intensity threshold. The results for 6-nm particles with 5 wt% or 10 wt% concentrations were not studied here because these cases are far out of the independent scattering zone.

4.3. Modeling results

4.3.1. Independent scattering

The Mie scattering theory can be used to calculate the absorption efficiency of a single particle only when the concentration of the particles in the droplet is sufficiently diluted, and the clearance between particles is large enough so that the scattering interference is negligible. Therefore determining the scattering pattern (either independent or dependent scattering) is crucial for the modeling work. It also has helped us choose the appropriate particle concentrations for the experiment at varying particle sizes so that the independent scattering assumption holds.

For a colloid, the distance between the centers of two particles is

$$L = \sqrt[3]{\frac{6}{\pi}} N_p^{-1/3} = 1.2407 N_p^{-1/3} \tag{10}$$

And the clearance between two particles is

$$C = L - d_p \tag{11}$$

where N_p is the particle number density, and d_p is the particle diameter.

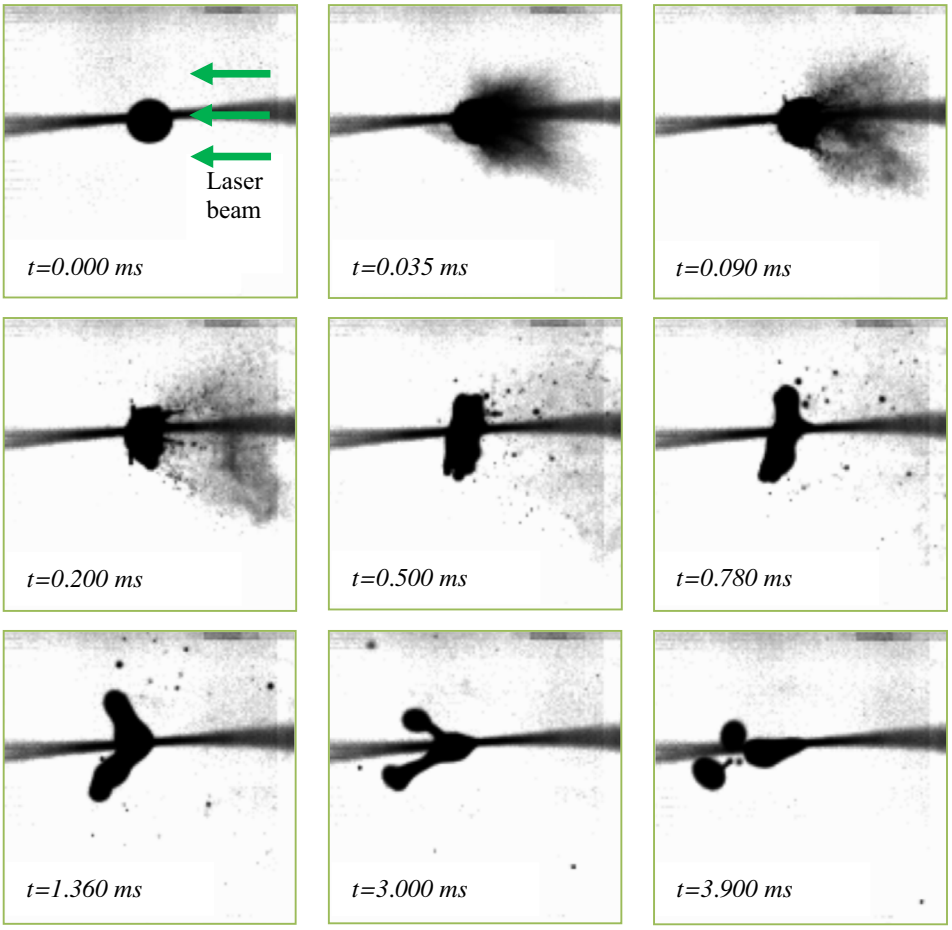

Fig. 4. Droplet breakup process.

Table 1
Laser-induced water droplet breakup thresholds.

Reference	Laser wavelength (μm)	Laser duration (ns)	Droplet material	Droplet diameter (μm)	Intensity threshold (W/cm^2)
[3]:No fiber	10.591	~400	Distilled water	(12.2–52.1)	$(1.43–2.34) \times 10^7$
			Boiled water	40.8	1.81×10^7
			Tap water	41.0	1.47×10^7
[5]:No fiber	0.532	10	Water	35	10^9
Present study: fiber-suspended	0.532	10	Deionized water	$(1–2) \times 10^3$	10^9

The experimental results from Brewster and Tien [25] showed that the independent scattering can be assumed as long as the interparticle clearance is greater than about 0.3 wavelengths ($C/\lambda > 0.3$). Based on this rule, we plotted all the critical points of the particle mass fraction and particle sizes that satisfy $C/\lambda > 0.3$ for a wavelength of 532 nm, as shown in Fig. 8. The entire domain is divided into two regions by this curve. Above the curve, we have $C/\lambda > 0.3$ and thus dependent scattering can be assumed. Below the curve, we have $C/\lambda > 0.3$ and thus independent scattering can be assumed. The particle mass fraction (1, 5 and 10 wt%) we chose in the experiments for 100 nm and 20 μm particles are categorized in the independent scattering region. For 6 nm particles, however, to fall in the independent scattering zone the particle mass fraction has to be very low (about 0.01 wt%). Studying such low concentration suspensions would not provide useful insights on practical coal-in-water fuels. As a result, we chose to use 1 wt% mass fraction for 6 nm particles but still assumed independent scattering in the modeling. The limitations and the consequence associated with this assumption will be discussed later in Section 4.3.3.

4.3.2. Absorption efficiency of the particle

For independent scattering, the amount of energy that can be absorbed by a single particle is mainly determined by the particle size, the complex refractive indices of the particle and the medium. To be consistent with the experiment, the wavelength of the incident laser beam was set to 532 nm. The complex refractive indices for the carbon and water are $m_1 = 1.7 + 0.8i$ and $m_2 = 1.327 + 0.0000029i$, respectively [26]. Note the complex refractive index of carbon is for the bulk material; it may not be accurate when the particle size decreases to nanoscale due to quantum confinement effect.

Fig. 9 shows the absorption efficiency of the particle as a function of the particle size. The correlation between the absorption efficiency and the particle size is in resonant mode, and this is determined by the Mie scattering theory [27,28]. At a certain

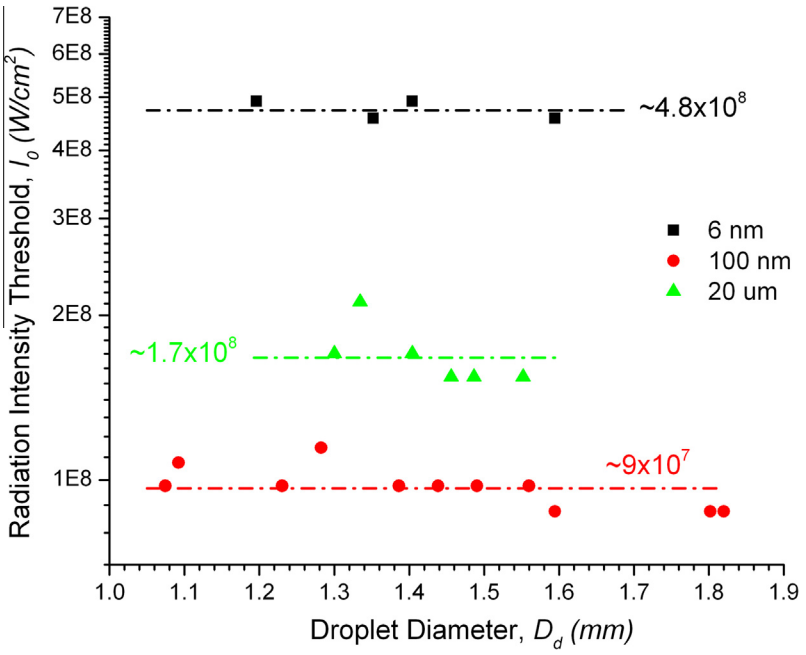

Fig. 5. Measured radiation-intensity threshold required for droplet breakup as a function of droplet diameter for three particle sizes 6 nm, 100 nm, and 20 μm, respectively. The particle concentration is 1 wt%. The dash lines represent an averaged value of the radiation-intensity threshold for each particle size.

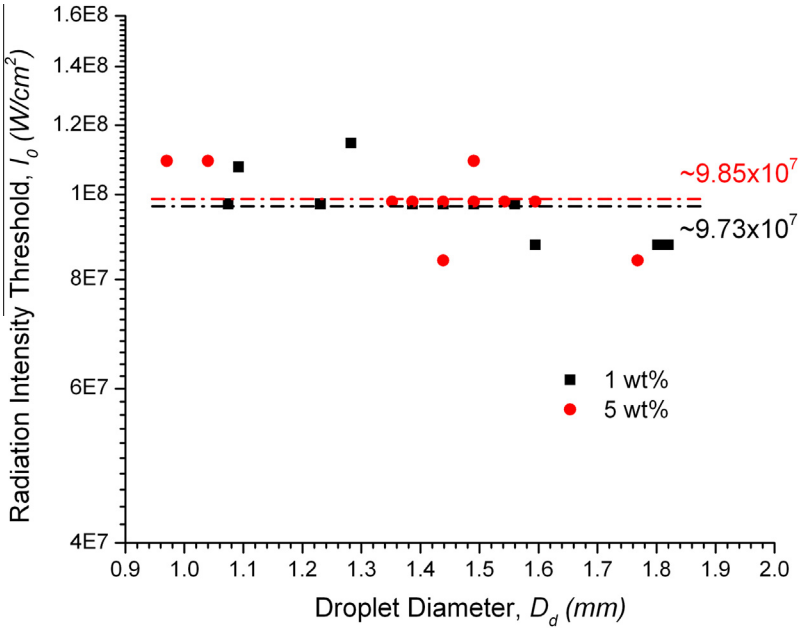

Fig. 6. Measured radiation-intensity threshold required for droplet breakup as a function of droplet diameter for two particle concentrations, 1 and 5 wt%, respectively. The particle size is 100 nm. The dash lines represent an averaged value of the radiation-intensity threshold for each particle concentration.

particle size, the absorption efficiency is solely a function of the complex refractive indexes [29]. In Fig. 9, the absorption efficiency increases for nano-sized particles and peaks at 1.18 when the particle size is 0.9 μm. After that, the absorption efficiency starts to decrease and becomes stable at around 0.94 when the particle size is larger than 30 μm.

4.3.3. Calculated radiation-intensity threshold

The droplet breakup occurs when the temperature of the water at the particle–fluid interface exceeds its maximum superheat temperature. The radiation-intensity threshold for droplet breakup can be calculated by varying the radiation intensity until the water temperature reaches 578 K. The droplet was assumed to be illuminated by a 10-ns laser pulse with 532 nm wavelength, and the particle concentration in the droplet is 1 wt%. Fig. 10 shows the calculated radiation-intensity threshold as a function of particle size. The results show that the radiation-intensity threshold decreases from 1 nm to 300 nm and then increases. This trend is consistent with the experimental results. Moreover, the calculated and measured radiation-intensity threshold agrees very well for the droplets with 20-μm particles (1.7×10^8 W/cm^2). The agreement, however, is less satisfactory for the droplets with 100-nm and 6-nm particles (1.9×10^7 vs. 9×10^7 W/cm^2 for 100-nm; 3.5×10^9 vs. 4.8×10^8 W/cm^2 for 6-nm). The deviation increases

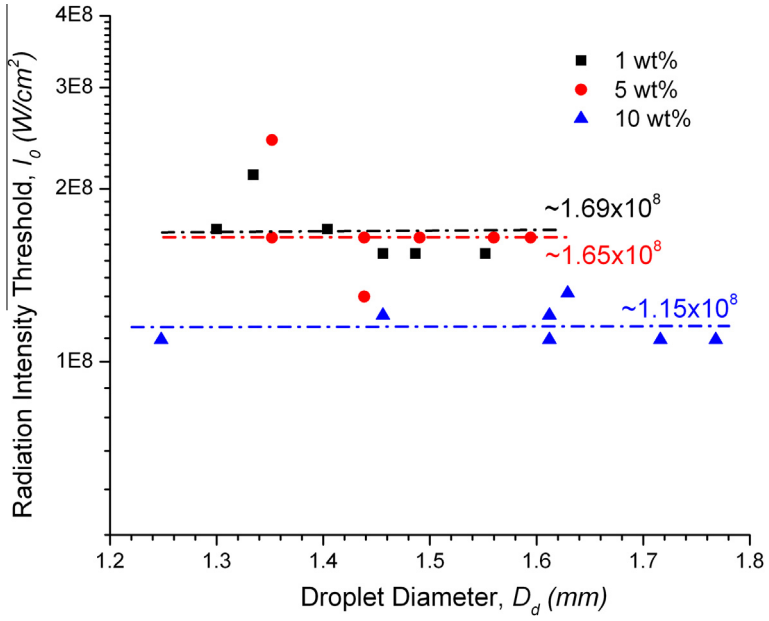

Fig. 7. Measured radiation-intensity threshold required for droplet breakup as a function of droplet diameter at three particle concentrations. The particle size is 20 μm. The dash lines represent an averaged value of the radiation-intensity threshold for each particle concentration.

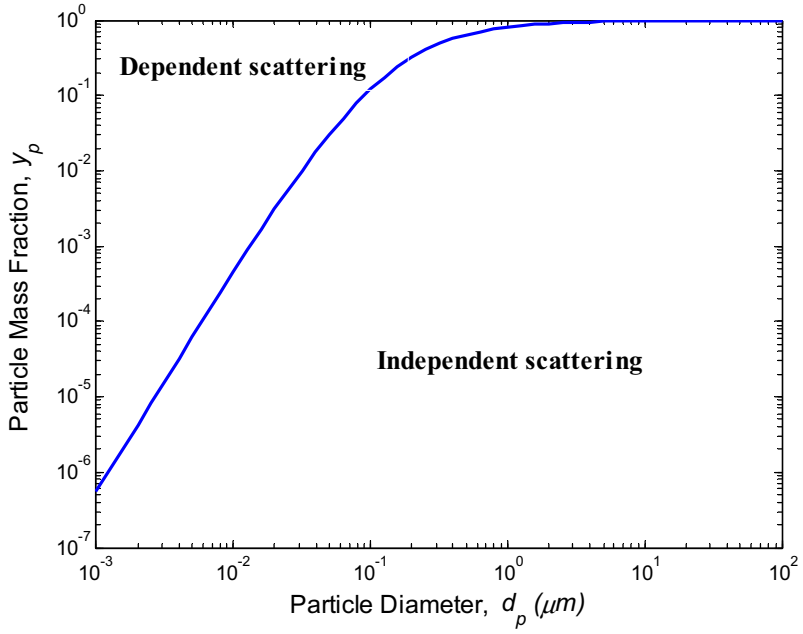

Fig. 8. Independent scattering region and dependent scattering region as functions of the particle diameter and the particle mass fraction for 532 nm wavelength.

as the particle size decreases. Also we can see that under a fixed radiation intensity of 1×10^8 W/cm^2 and heating time of 10 ns, only the droplets with particles in the size range of 36 nm to 11 μm can breakup.

The calculated radiation intensity threshold has the lowest value around 300 nm, and this is a result of the combined effects of the absorption efficiency of the particles and the thermal conduction rate between the particles and the surrounding water. The thermal conduction rate from the particle surface to the surrounding water is much higher at smaller particle size because of its higher surface-to-volume ratio. However, as shown in Fig. 9, the absorption efficiency is much lower when the particle size is less than 100 nm. Therefore the lowest radiation intensity threshold is presented at 300 nm.

As an example, Fig. 11 shows the temperature profiles of the particle and the water on the interface for 20 μm particles under two radiation intensities. The temperature profiles for the cases with 6 nm and 100 nm particles are similar to those with 20 μm particles and thus are not shown here. For both cases in Fig. 11, the particle temperatures peak at 10 ns because of the radiation absorption, and start to decrease after 10 ns due to the thermal conduction between the two phases. When the radiation intensity is at 1.7×10^8 W/cm^2, which is the threshold value for 20 μm particle, the water temperature on the interface keeps increasing and reaches 578 K around 100 ns. When the radiation intensity is at 0.5×10^8 W/cm^2 which is lower than the threshold, the water temperature on the interface increases and becomes stable at 400 K. And in this case, the breakup will not occur.

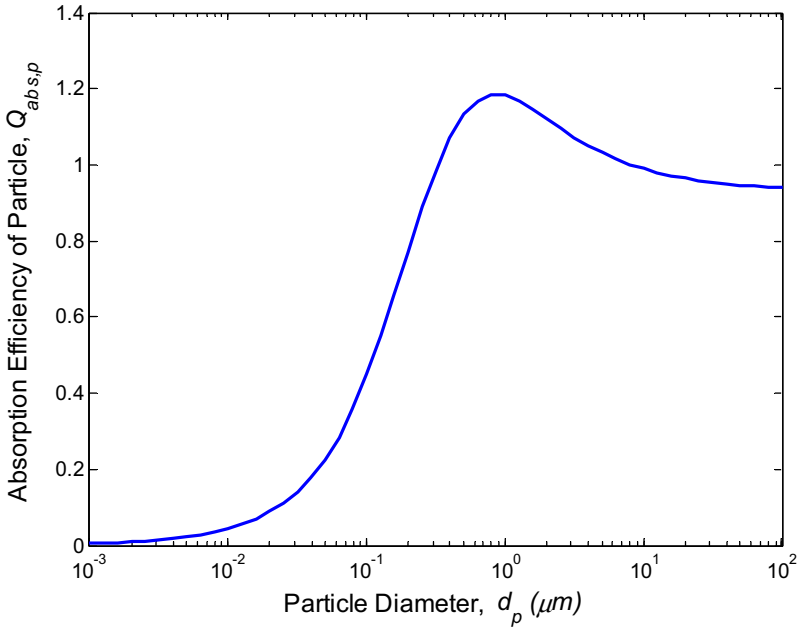

Fig. 9. Calculated absorption efficiency of the particles as a function of particle diameter.

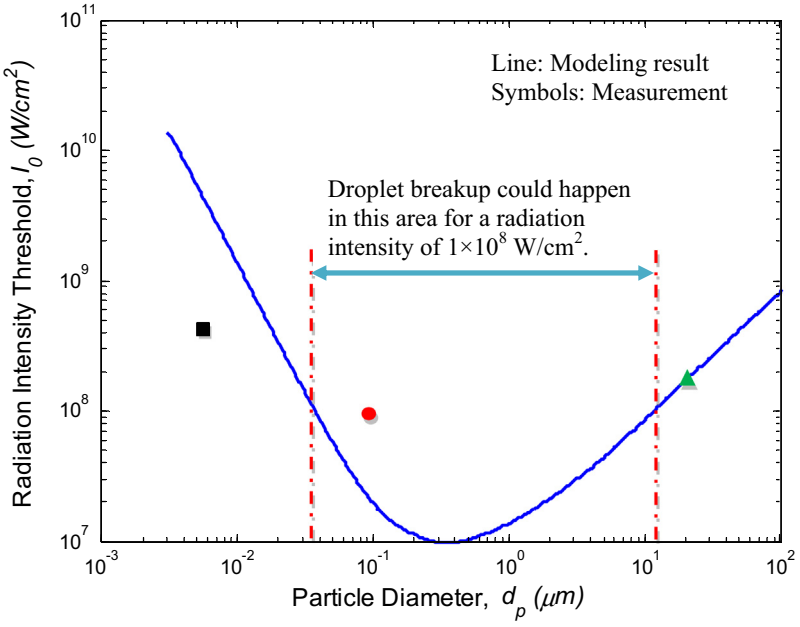

Fig. 10. Calculated and measured radiation-intensity threshold for droplet breakup as a function of particle size. The particle concentration is 1 wt%. For radiation intensity of 1×10^8 W/cm^2, the droplet breakup could happen only for the particle sizes between the two red lines. (For interpretation of the references to color in this figure legend, the reader is referred to the web version of this article.)

As mentioned earlier, for 6 nm particles, we considered 1 wt% concentration, which falls in the dependent scattering zone. But independent scattering assumption was adopted in the modeling. For dependent scattering, which multiple scattering occurs between particles suspended in the droplet, it would lower the radiation intensity threshold required to cause a droplet breakup. In other words, if dependent scattering had been considered in the modeling, the discrepancy between the experimental and the modeling results for 6 nm particles in Fig. 10 would be smaller.

In addition, recall that the refractive index of bulk carbon ($m_1 = 1.7 + 0.8i$) was used for all particles with different sizes. This assumption holds for particle size larger than 3 μm as found in [26], but it may be inaccurate for nano-sized particles, especially when the size is down to only a few nanometers [30]. Studies have shown that the complex refractive index can be significantly different at nano-scale and at bulk scale because of the quantum confinement effect [31], which can be observed when the particle size is too small to be comparable to the wavelength of the electron.

4.3.4. Sensitivity analysis

To examine how the calculated radiation-intensity threshold is influenced by the uncertainties associated with the complex refractive index of the particles at various sizes, we conducted a

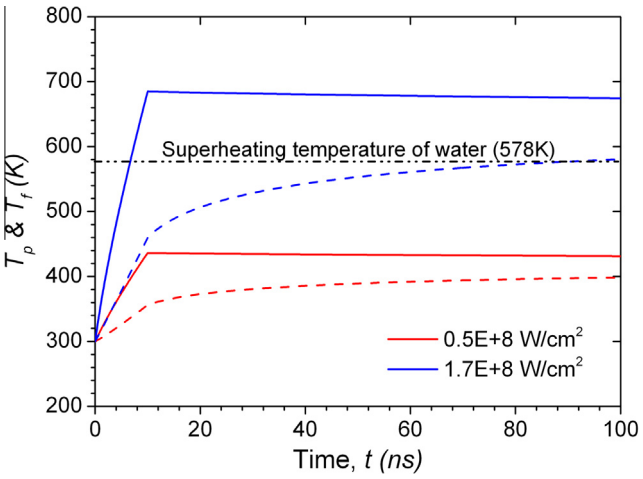

Fig. 11. Computed temperature profiles of the 20 μm particle and the surrounding water on the two-phase interface under different radiation intensity. The solid lines are the particle temperatures and the dash lines are the water temperatures.

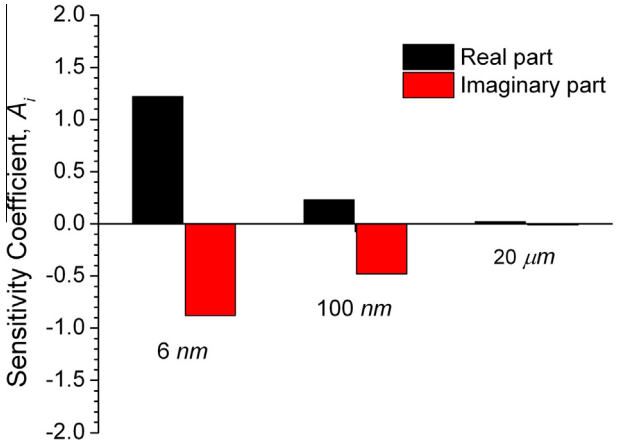

Fig. 12. Sensitivity coefficients of the calculated radiation-intensity threshold with respect to the real and imaginary parts of the complex refractive index of the particles (carbon).

sensitivity analysis on the radiation-intensity threshold with respect to the real and imaginary parts of the complex refractive index. The sensitivity coefficient was defined as

$$A_i = \frac{R_i}{y}\frac{\Delta y}{\Delta R_i} \tag{12}$$

where A_i is the sensitivity coefficient, y is the examined parameter (the radiation-intensity threshold), and R_i is the model parameters (both the real and imaginary parts of the complex refractive index of the particle). The sensitivity coefficient was obtained by artificially perturbing one of the model parameters by 10% while keeping the other one fixed.

The sensitivity coefficients with respect to the real and imaginary parts of the refractive index of the particle (carbon) are shown in Fig. 12. When the particle size is 20 μm, both the real and imaginary parts of the complex refractive index of the particle have little impact on the radiation-intensity threshold. However, when the particle size decreases to nanoscale, the influences of both the real and imaginary parts of the complex refractive index of the particle become significant. This means that the modeled results largely depend on the accuracy of the refractive index for nano-sized particles. Unfortunately, such data in the nano regime, which are particle-size dependent, are not available currently in the literature. Furthermore, the sensitivity coefficients with respect to the imaginary part have negative values. This is because the radiation absorption is proportional to the imaginary part of the complex refractive index. An increase in the imaginary part will lead to a higher radiation absorption and will require a lower radiation-intensity threshold for droplet explosion.

5. Conclusions

This paper is one of the first to study radiation-induced droplet breakup of micro- and nano-dispersed coal-in-water colloidal suspensions using a combined experimental and modeling approach. The results show that the breakup mechanism, quite different from that for pure water, is due to the radiation absorption of individual carbon particles suspended in the droplet. The threshold radiation intensity required for droplet breakup does not depend on droplet size, but varies significantly with various particle sizes. Furthermore, the threshold radiation intensity does not depend on particle concentration unless the concentration becomes high, for which the multiple scattering effect will become more significant leading to a lower radiation-intensity threshold. .

A theoretical model that considered radiation absorption and scattering by the droplet and by the particles along with heat conduction between the particles and the surrounding water in a thin nanoscale thermal layer was also developed to understand the mechanism of droplet breakup and to predict the threshold radiation intensity. The predicted and measured threshold radiation energy intensities show the same trend for various particle sizes. Both decrease first, and they then increase as the particle size increases. The results show that the radiation-intensity threshold was determined by a combined effect of the absorption efficiency of the particles and the thermal conduction rate between the particles and the surrounding water.

Lastly, the predicted and measured threshold radiation energy intensities agree well for micron-sized particles. The agreement, however, is less satisfactory when the particle size decreases to nanoscale. One reason for the discrepancy is that independent scattering assumption used in the modeling was not valid for the concentrations studied – indeed dependent scattering occurred which lowered the radiation intensity threshold. Additionally, a sensitivity analysis was performed to examine how the predicted threshold radiation intensity depends on the accuracy of the complex refractive index of the particles. The results show that both the real and imaginary parts of the complex refractive index of the particle have little impact on the radiation-intensity threshold when the particle is micron-sized. However, when the particle size decreases to nano-scale, the influences of both the real and imaginary parts of the complex refractive index of the particle become significant.

Conflict of interest

None declared.

Acknowledgment

This work has been supported by the National Science Foundation with Dr. Ruey-Hung Chen as the technical monitor.

References

[1] I. Belousova, N. Mironova, M. Yur'ev, Theoretical investigation of nonlinear limiting of laser radiation power by suspensions of carbon particles, Opt. Spectrosc. 94 (1) (2003) 86–91.

[2] R.W. Breault, Gasification processes old and new: a basic review of the major technologies, Energies 3 (2) (2010) 216–240.
[3] R.G. Pinnick, A. Biswas, R.L. Armstrong, S.G. Jennings, J.D. Pendleton, G. Fernáandez, Micron-sized droplets irradiated with a pulsed CO_2 laser: measurement of explosion and breakdown thresholds, Appl. Opt. 29 (7) (1990) 918–925.
[4] R.K. Chang, J.H. Eickmans, W.-F. Hsieh, C.F. Wood, J.-Z. Zhang, J.-B. Zheng, Laser-induced breakdown in large transparent water droplets, Appl. Opt. 27 (12) (1988) 2377–2385.
[5] J.Z. Zhang, J.K. Lam, C.F. Wood, B.T. Chu, R.K. Chang, Explosive vaporization of a large transparent droplet irradiated by a high-intensity laser, Appl. Opt. 26 (22) (1987) 4731–4737.
[6] D.J. Maloney, J.F. Spann, Secondary atomization of coal–water fuel droplets resulting from exposure to intense radiant heating environments, Abstr. Pap. Am. Chem. S 191 (1986). 18-Fuel.
[7] D.J. Maloney, J.F. Spann, Evaporation agglomeration and explosive boiling characteristics of coal–water fuels under intense heating conditions, Symp. (Int.) Combust. 22 (1) (1989) 1999–2008.
[8] J.F. Spann, D.J. Maloney, W.F. Lawson, K.H. Casleton, Response of 2-phase droplets to intense electromagnetic-radiation, Appl. Opt. 32 (12) (1993) 2152–2158.
[9] D.Y. Byun, S.W. Baek, J.H. Cho, Microexplosion of aluminum slurry droplets, Int. J. Heat Mass Transfer 42 (24) (1999) 4475–4486.
[10] Y.A. Gan, L. Qiao, Combustion characteristics of fuel droplets with addition of nano and micron-sized aluminum particles, Combust. Flame 158 (2) (2011) 354–368.
[11] K. Miyasaka, C.K. Law, Combustion and agglomeration of coal–oil mixtures in furnace environments, Combust. Sci. Technol. 24 (1–2) (1980) 71–82.
[12] G.A. Nunez, M.I. Briceno, D.D. Joseph, T. Asa, Colloidal coal in water suspensions, Energy Environ. Sci. 3 (5) (2010) 629–640.
[13] N.T. Tong, Photophoretic force in free molecule and transition regimes, J. Colloid Interface Sci. 43 (1) (1973) 78–84.
[14] N.T. Tong, Experiments on photophoresis and thermophoresis, J. Colloid Interface Sci. 51 (1) (1975) 143–151.
[15] D.A.G. Bruggeman, Calculation of various physics constants in heterogenous substances. I. Dielectricity constants and conductivity of mixed bodies from isotropic substances, Ann. Phys.-Berlin 24 (7) (1935) 636–664.
[16] M. Sitarski, On the feasibility of secondary atomization of small slurry droplets exposed to intense thermal-radiation, Combust. Sci. Technol. 54 (1–6) (1987) 177–201.
[17] G. Mie, Articles on the optical characteristics of turbid tubes, especially colloidal metal solutions, Ann. Phys.-Berlin 25 (3) (1908) 377–445.
[18] C.F. Bohren, D.R. Huffman, Absorption and Scattering of Light by Small Particles, John Wiley and Sons, 1983.
[19] C. Mätzler, MATLAB Function for MIE Scattering and Absorption, 2002.
[20] A. Plech, V. Kotaidis, S. Gresillon, C. Dahmen, G. von Plessen, Laser-induced heating and melting of gold nanoparticles studied by time-resolved X-ray scattering, Phys. Rev. B 70 (19) (2004).
[21] O.M. Wilson, X.Y. Hu, D.G. Cahill, P.V. Braun, Colloidal metal particles as probes of nanoscale thermal transport in fluids, Phys. Rev. B 66 (22) (2002).
[22] S.T. Huxtable, D.G. Cahill, S. Shenogin, L. Xue, R. Ozisik, P. Barone, M. Usrey, M.S. Strano, G. Siddons, M. Shim, Interfacial heat flow in carbon nanotube suspensions, Nat. Mater. 2 (11) (2003) 731–734.
[23] Z. Ge, Nanoscale Thermal Transport at Solid–Liquid Interfaces, University of Illinois, 2006.
[24] G. Sun, C.W. Trueman, Unconditionally stable Crank–Nicolson scheme for solving two-dimensional Maxwell's equations, Electron. Lett. 39 (7) (2003) 595–597.
[25] M.Q. Brewster, C.L. Tien, Radiative-transfer in packed fluidized-beds – dependent versus independent scattering, J. Heat Trans. – Trans. ASME 104 (4) (1982) 573–579.
[26] A.B. Pluchino, S.S. Goldberg, J.M. Dowling, C.M. Randall, Refractive-index measurements of single micron-sized carbon particles, Appl. Opt. 19 (19) (1980) 3370–3372.
[27] H.C.v.d. Hulst, Light Scattering: By Small Particles, John Wiley and Sons, Chapman and Hall, New York, London, 1957.
[28] C. Bohren, D. Huffman, Absorption and Scattering of Light by Small Particles, Wiley science paperback series, Wiley-VCH, 1998.
[29] J. Popp, M. Lankers, K. Schaschek, W. Kiefer, J.T. Hodges, Observation of sudden temperature jumps in optically levitated microdroplets due to morphology-dependent input resonances, Appl. Opt. 34 (13) (1995) 2380–2386.
[30] A. Eremin, E. Gurentsov, E. Popova, K. Priemchenko, Size dependence of complex refractive index function of growing nanoparticles, Appl. Phys. B – Lasers Opt. 104 (2) (2011) 285–295.
[31] Y.K. Chang, H.H. Hsieh, W.F. Pong, M.H. Tsai, F.Z. Chien, P.K. Tseng, L.C. Chen, T.Y. Wang, K.H. Chen, D.M. Bhusari, J.R. Yang, S.T. Lin, Quantum confinement effect in diamond nanocrystals studied by X-ray-absorption spectroscopy, Phys. Rev. Lett. 82 (26) (1999) 5377–5380.